Relative Partial Cross Sections for Single, Double, and Triple Photoionization of C_{60} and C_{70}

Koichiro Mitsuke,*,†,‡ Hideki Katayanagi,†,‡ Bhim P. Kafle,‡ Chaoqun Huang,† Hajime Yagi,† Md. Serajul I. Prodhan,‡ and Yoshihiro Kubozono§

The Institute for Molecular Science, and Graduate University for Advanced Studies, Myodaiji, Okazaki 444-8585, Japan, and Department of Chemistry, Faculty of Science, Okayama University, Okayama 700-8530, Japan

Received: April 3, 2007; In Final Form: June 12, 2007

Partial cross sections for the photoion formation from C_{60} and C_{70} were determined from the yields of singly, doubly, and triply charged ions which were measured by mass spectrometry combined with tunable synchrotron radiation at $h\nu = 25-120$ eV. The dependence of the detection efficiencies on the mass-to-charge ratio was evaluated by using the formula proposed by Twerenbold et al. Corrections of the detection efficiency were found to be critical for obtaining accurate partial cross sections for photoionization of fullerenes. Revisions were made of the partial cross-section curves for single and double photoionization of C_{60} and C_{70}. The curve for triple photoionization of C_{70} was newly proposed. The ratios between the cross sections for double and single photoionization increase with $h\nu$ and reach saturated values of 0.78 at 85 eV for C_{60} and ∼1.3 at 100 eV for C_{70}. In contrast, the ratios at 120 eV between the cross sections for triple and single photoionization of C_{60} and C_{70} amount to 0.14 and ∼0.38, respectively. The formation mechanism of multiply charged fullerene ions was discussed in terms of valence-electron excitation to antibonding unoccupied orbitals and/or spherical standing waves inside the cavity of a fullerene. This excitation could be followed by Spectator Auger processes and transmission of the excess electronic energy among numerous vibrational degrees of freedom.

Introduction

Dynamics of excitation and ionization of fullerenes have attracted increasing attention because of observation of unique phenomena due to high symmetry of fullerenes, such as collective plasmon oscillation of valence electrons[1] and interference between the standing waves of the ionized electron inside a fullerene cage.[2] However, difficulties in acquiring a sufficient quantity of the sample have hindered many investigators in acquiring even fundamental spectroscopic information in the extreme UV region. This situation is now being altered since the techniques of synthesis, isolation, and purification have advanced so rapidly that appreciable amounts of fullerenes can be readily gained.

Our group has measured the yields of ions produced from C_{60} and C_{70} by time-of-flight (TOF) mass spectrometry, determining relative partial cross sections for production of singly and doubly charged ions. Kou et al.[3] have demonstrated that the ratio $\sigma(60,2+)/\sigma(60,+)$ between the cross sections for double and single photoionization of C_{60} increases with increasing photon energy $h\nu$ and asymptotically reaches 2.1−2.3 at $h\nu > 80$ eV. A similar trend could be seen for C_{70} and the corresponding ratio $\sigma(70,2+)/\sigma(70,+)$ was 3−4, though there exists some scatter of the data points. These ratios for C_{60} and C_{70} are 1 to 2 orders of magnitude higher than those documented by many references dealing with photoionization of ordinary molecules.[4,5] Furthermore, the yields of fragment ions C_{60-2n}^+ and C_{70-2n}^+ ($n \geq 1$) are markedly lower than those of the parent ions.[6,7] The above observations are well-interpreted as that the excess internal energy is transmitted so quickly among enormous vibrational degrees of freedom that unimolecular reactions, such as direct dissociation, electronic predissociation, or coulomb explosion, are substantially suppressed and the lifetime of the parent ions is extended beyond the order of a millisecond. In other words, the overall rate of the internal conversion followed by intramolecular vibrational redistribution (IVR) may overwhelm that of dissociation into two or more singly charged fragments.

Kou et al. have mentioned that no correction has been made for the relative detection efficiency η of the ion detector that they employed.[3] This statement was based on the fact that the ratios between the yield of Ar^+ and that of Ar^{2+} at $h\nu = 70$, 80, and 90 eV were in good agreement with the values in the literature[8] within an experimental accuracy. However, several authors[9−13] have argued rapid decrease in η with increasing mass-to-charge ratio m/z at $m/z > 150$, when a TOF mass spectrometer is equipped with a conventional ion detector which operates with normal voltage settings. Here, the "conventional ion detector" usually refers to a secondary electron multiplier comprising two microchannel plates (MCPs), while "normal voltage settings" means applying the full bias voltage of ca. −2 kV across the two plates and grounding the output of the MCP assembly. The experimental setups of Kou et al. fulfilled these conditions, so it is likely that η is far from saturation and crucially dependent on m/z of the fullerene ion.

Reinköster et al.[14] have reported that $\sigma(60,2+)/\sigma(60,+)$ reaches a plateau of ∼0.6 at $h\nu = 62-130$ eV. This plateau ratio was about one-third of the asymptotic ratio given by Kou et al.[3] In 2006 Juranic et al.[15] performed a similar measurement up to $h\nu = 280$ eV and obtained a value of 0.65 at $h\nu = 100$ eV where the $\sigma(60,2+)/\sigma(60,+)$ curve makes a local maximum.

† The Institute for Molecular Science.
‡ Graduate University for Advanced Studies.
§ Okayama University.

10.1021/jp0726034 CCC: $37.00
Published on Web 08/07/2007

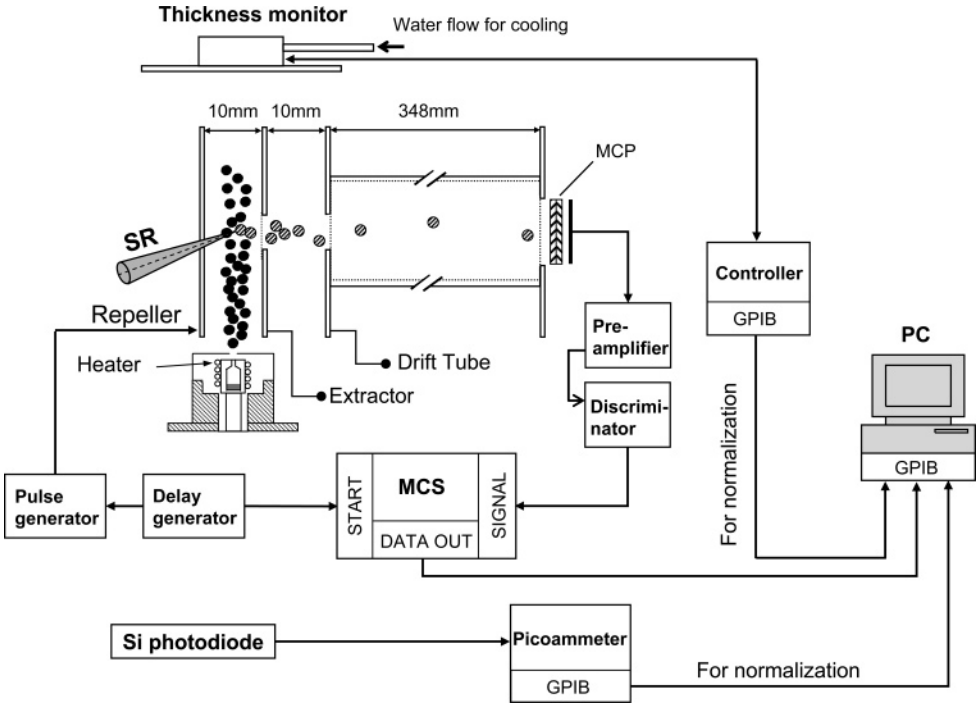

Figure 1. Schematic diagram of the apparatus. SR, monochromatized synchrotron radiation; MCS, multichannel scaler; MCP, microchannel plate electron multiplier; PC, personal computer.

This value is again about one-third of the asymptotic ratio given by Kou et al. Reinköster et al. and Juranic et al. employed secondary electron multipliers containing three MCPs. They claimed that saturation of η can almost be realized with such ion detectors[14,15] because the pulse height of the detector signal is shifted to much higher values and because a bias voltage lower than -3 kV can be applied to the entrance surface of the MCP assembly.

Even if mass spectrometric study is made with a conventional ion detector composed of two MCPs, one may evaluate $\sigma(60,2+)/\sigma(60,+)$ to a good approximation by examining the variation of η as a function of either impinging velocity, momentum, or kinetic energy. In 2001 Twerenbold et al. reported an empirical functional form of velocity dependence of η by comparison of mass spectra taken with conventional ion detectors and those with a single-molecule sensitive cryo-detector.[9] They demonstrated the validity of the formula[9,10] over a wide velocity range from 5 to 62 km s^{-1} or a wide mass range from 1.5 to 135 kDa.

In the present paper, we investigate the yield curves of ions in charge states of $z = 1-3$ produced from C_{60} and C_{70}, with particular attention being paid to the ratios between the partial cross sections for multiple and single photoionization. Reliable η can be derived from the formula of Twerenbold et al. and introducing the correction of η may lead to reasonable modification of our previous results[3] of these ratios. We will compare our revised partial cross sections for C_{60} with those determined by other workers.[3,14−16] On the other hand, no data has been available on the partial cross sections for multiply charged ions from C_{70} over a wide photon energy range. Next, we will discuss a universal formation mechanism of multiply charged ions which is consistent with the $h\nu$ dependence of the observed partial cross-section curves, by taking into account primary photoexcitation to high-lying resonance states and relaxation of the excess energy in excited fullerene ions.

Experimental Section

Apparatus and Sample Preparation. All the measurements have been carried out at the bending magnet beamline BL2B constructed in the UVSOR synchrotron radiation facility in Okazaki, equipped with an 18 m spherical grating monochromator of Dragon type.[17,18] The monochromator has been designed to cover the $h\nu$ range 25−150 eV by using three gratings: G1 (2400 lines mm^{-1}, $R = 18$ m) at 80−150 eV; G2 (1200 lines mm^{-1}, $R = 18$ m) at 40−100 eV, and G3 (2400 lines mm^{-1}, $R = 9.25$ m) at 25−50 eV.[19]

The light monochromatized by the grating G2 was subject to contamination of the second-order light. We estimated the $h\nu$ dependence of the percentage of the second-order light by measuring the ion yield spectrum of He at $h\nu = 40-100$ eV. The percentage was optimized as an adjustable parameter to reproduce the observed spectrum from the absorption cross section data[20] of He. For instance, the percentage at $h\nu = 45$ eV was found to be 22%. Alternatively, the percentage of the second-order light could be calculated based on the Kr^+ yield spectra of Kr in the vicinity of the $3d_{5/2}^{-1}\,5p^1$ resonance peaks appearing at 45.6 and 91.2 eV, with the aid of the reported partial photoionization cross sections[21] of Kr at ∼45 and ∼90 eV. The resultant percentage was 23% at ∼45 eV, which accords well with the value obtained using the ion yield spectrum of He.

Figure 1 shows the side view of the apparatus. The samples of C_{60} and C_{70} with the purity of 99.98% and 99.5%, respectively, were purchased (Matsubo) and further purified by eliminating the organic solvent such as benzene or toluene through heating the samples 1 day in a vacuum at 200 °C. The powder of C_{60} or C_{70} loaded in a quartz sample holder was discharged as a molecular beam from an exit hole with a diameter of 1.0 or 2.5 mm. The sample holder was heated up to approximately 670−770 K. Monochromatized synchrotron radiation was focused onto the fullerene beam and photoions of fullerenes were produced. A pulsed voltage rising from the ground level to +80 V was applied to the ion repeller electrode

as a start trigger for the time-of-flight (TOF) measurement. The duration and frequency of this pulse voltage were 4.5 μs and 10−20 kHz, respectively. The photoions were extracted by the pulsed electric field, mass-separated by a double-focusing TOF mass spectrometer, and detected with a secondary electron multiplier comprising two MCPs (diameter 27 mm; Hamamatsu, F1552). The entrance surface of the front MCP was biased to the voltage of −2.1 kV, while the exit surface of the back MCP was grounded. The signal from MCP was processed by a conventional pulse counting system and a multichannel scaler (FastComtec, 8867). Ion signal counts were integrated over the respective mass peaks. To obtain an ion yield, the fluxes of synchrotron radiation and molecular beams were monitored throughout the measurement.[18,22] First, the photon flux was estimated by measuring the photocurrent from a silicon photodiode (IRD, AXUV-100). Second, a crystal-oscillator surface thickness monitor (Inficon, XTM/2) was employed to measure the flux of the molecular beam and evaluate fullerene density in the ionization region. A photoion yield spectrum was constructed by normalizing the integrated ion counts at each $h\nu$ to the photon and molecular-beam fluxes and by collecting the normalized counts consecutively with changing $h\nu$. The experimental setup for photoionization mass spectrometry of the fullerene family has been described in detail elsewhere.[18,22,23]

Derivation of the Relative Partial Cross Sections. The procedure to calculate a partial cross section for the photoion formation from the fullerene is essentially the same as that employed in our previous paper[22] for evaluation of the cross sections of C_{60}. In the present paper we improved this procedure to obtain more accurate cross sections by introducing correction of relative detection efficiencies of the MCP ion detector. The absolute partial cross section for the formation of photoions in a charge state z from the C_k sample (k = 60 and 70) can be expressed as

$$\sigma_{abs}(k,z+) = R(k,z+)/\Phi nL\eta_{abs}(C_k^{z+})f\tau \qquad (1)$$

Here, $R(k,z+)$ is the signal count rate of all the ions in a charge state z produced from the fullerene C_k, Φ is the photon flux of synchrotron radiation, n is the number density of C_k in the ionization region, L is the length of the ionization volume along the light path, $\eta_{abs}(C_k^{z+})$ is the absolute detection efficiency of the apparatus for C_k^{z+}, f is the repetition rate of the pulsed electric field applied to the ionization region, and τ is the average residence time of the ions in the ionization volume without the pulsed electric field. To a first approximation τ is proportional to the inverse of the average flow speed $\bar{v}$ of the neutral C_k beam, while n is proportional to (a) the mass deposition rate D of the thickness monitor, (b) the inverse of $\bar{v}$, and (c) the inverse of the mass m of C_k. Since the quantities L and f are kept constant through all the measurements, eq 1 can be written as

$$\begin{aligned}\sigma_{abs}(k,z+) &\propto R(k,z+)\, m\bar{v}^2/\Phi D\eta(C_k^{z+}) \\ &\propto R(k,z+)T/\Phi D\eta(C_k^{z+}) = \\ &\qquad Y(k,z+)T/\eta(C_k^{z+}) \equiv \sigma(k,z+) \qquad (2)\end{aligned}$$

where T denotes the temperature of the sample holder and $\sigma(k,z+)$ does a partial cross section for formation of the ions with a charge z from C_k. Derivation of the relative detection efficiency $\eta(C_k^{z+})$ of the MCP will be discussed later. The normalized count rate $Y(k,z+) = R(k,z+)/\Phi D$ is equal to the ion yield if variation of T is negligible during a given experimental run, and thus the $\sigma(k,z+)$ curve can be obtained by plotting $Y(k,z+)/\eta(C_k^{z+})$ as a function of $h\nu$. Adopting eq 2 to the ions in different charge states allows us to calculate the ratio between the partial cross sections for the multiply and singly charged ions as

$$\frac{\sigma(k,z+)}{\sigma(k,+)} = \frac{R(k,z+)}{R(k,+)}\frac{\eta(C_k^{+})}{\eta(C_k^{z+})} \qquad (k = 60, 70;\ z = 2, 3) \qquad (3)$$

This ratio was not affected by the variation or fluctuation of Φ and D while $h\nu$ was being scanned because, at each $h\nu$, Φ and D values are common for all the fullerene ions produced in the C_k beam.

The detection efficiency of the TOF mass spectrometer depends on m/z of the detected ion. In the case of our apparatus the detection efficiency is found to be determined mainly by the m/z dependence of the efficiency of the secondary electron multiplier with two MCPs. One of the general expressions of the m/z dependence for such ordinary ion detectors is an empirical formula proposed by Twerenbold et al.[9,10] with regard to the ions with $m/z = 1.5 \times 10^3$ to 1.35×10^5. The relative detection efficiency η can be calculated from their formula

$$\eta = 1 - \exp\left(-\left(\frac{v}{53}\right)^{3.5}\right) \qquad (4)$$

where the saturated efficiency is assumed to be unity and v denotes the velocity, in units of km s^{-1}, of the ion impinging on the entrance surface of the MCP assembly. This equation was found to hold from $v = 5$ to $v = 62$ km s^{-1}. In a low m/z region their expression reproduces well the η values derived from the polynomial function of $m^{0.5}v^2$ proposed by Krems et al.[11] In a high m/z region eq 4 successfully predicts the data of η obtained by various research groups with different mass spectrometers. We assume from Figure 4 in ref 9 that the magnitude of the errors in eq 4 is at most ±10% at $v \geq$ 20 km s^{-1}.

To inspect the applicability of the formula to our setup, we have experimentally estimated η values of singly, doubly, and triply charged photoions produced from rare gases (Kr and Xe) and fulfilled the least-squares fit of η's to the proposed formula. Normalizing the signal counts by the photon fluxes and absolute sample pressures permits the η values to be compared between Kr and Xe. The partial cross sections for the formation of Kr^{z+} and Xe^{z+} (z = 1−3) are taken from the literature.[8] The photon energy was so chosen that the contamination of the second-order light is negligible. The rare gas vapor was admitted to the vacuum chamber through a needle valve and its pressure was monitored with an ionization gauge which had been calibrated beforehand by a capacitance manometer. The gas pressure was postulated to be almost uniform inside the vacuum chamber. The experimental data points of η of Kr^{z+} and Xe^{z+} were fitted well to the formula of Twerenbold et al.,[9] so we concluded that the formula can properly explain the detection efficiency of our TOF spectrometer.

Relative detection efficiencies $\eta(C_k^{z+})$ for C_{60}^{z+} and C_{70}^{z+} were calculated using eq 4 from the acceleration voltages of our mass spectrometer (2.1 kV) and were summarized in Table 1. We made similar calculations by assuming the formula proposed by Krems et al.[11] and found that the two different formulas lead to $\eta(C_k^{z+})$ values close to each other. We utilized the values in Table 1 to correct the count rates of respective mass peaks as eq 2 to evaluate the partial cross sections for

TABLE 1: Relative Detection Efficiencies of Fullerene Ions C_k^{z+} ($z = 1$, 2, and 3)[a,b]

		detection efficiency		
k	ions	$\eta(C_k^{+})$	$\eta(C_k^{2+})$	$\eta(C_k^{3+})$
60	C_{60}^{z+}	5.81×10^{-2}	1.82×10^{-1}	3.36×10^{-1}
70	C_{70}^{z+}	4.47×10^{-2}	1.43×10^{-1}	2.69×10^{-1}

[a] Calculated by using the formula of Twerenbold et al.,[9] when the entrance surface of the front MCP is biased to the voltage of −2.1 kV and the exit surface of the back MCP is grounded. [b] Saturated efficiency is presumed to be unity.

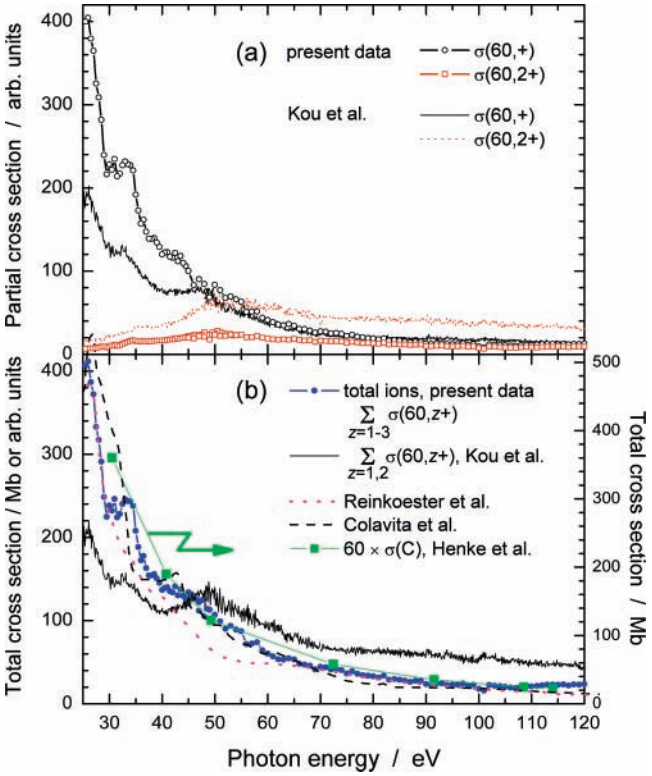

Figure 2. (a) Relative partial cross sections for single and double photoionization of C_{60}. The circle and square symbols designate $\sigma(60,+)$ and $\sigma(60,2+)$, respectively, of the present study. The solid and dotted curves indicate $\sigma(60,+)$ and $\sigma(60,2+)$ by Kou et al., respectively.[3] The two $\sigma(60,+)$ curves are normalized at $h\nu = 80$ eV. (b) Total photoionization cross section $\sigma_T(60)$ of C_{60}. Closed circles, the present results; solid curve, the sum of $\sigma(60,+)$ and $\sigma(60,2+)$ by Kou et al.;[3] dotted curve, experimental data[14] of $\sigma_T(60)$; dashed curve, theoretical total photoabsorption cross section;[16] closed squares, 60 times the total photoabsorption cross section[24] 60 × σ(C) of a C atom. The dotted[14] and dashed[16] curves are normalized to the present curve at $h\nu = 100$ eV. The 60 × σ(C) data and $\sigma_T(60)$ of the present study are plotted in a Mb unit against the right and left ordinates, respectively, while the other data in arbitrary units against the left ordinate.

formation of C_k^{z+} and concomitant fragment ions. Since the signal count rate of the fragment ion C_{k-2n}^{z+} rapidly decreases with increasing n (i.e., the number of C_2 units lost),[6,7] $\eta(C_k^{z+})$ has been substituted for the detection efficiencies of the C_{k-2n}^{z+} fragments ($n \geq 1$).

Results and Discussion

Partial Cross Sections for Single and Multiple Photoionization of C_{60}. Open circles and squares of Figure 2a show the relative partial cross sections $\sigma(60,+)$ and $\sigma(60,2+)$ for, respectively, single and double photoionization of C_{60} that were calculated using eq 2. It should be emphasized that each partial cross section includes the contribution of not only the parent but also fragment ions produced by the C_2-loss processes, so it is essentially equal to the cross section involving all the ionic species in a particular charge state. The solid and dashed curves in Figure 2a show $\sigma(60,+)$ and $\sigma(60,2+)$, respectively, reported by Kou et al.[3] in 2004. At $h\nu \geq 50$ eV the present $\sigma(60,2+)$ is about one-third as large as that by Kou et al. because the relation $\eta(C_{60}^{2+}) = 3.13\eta(C_{60}^{+})$ has been taken into account as discussed in the Experimental Section. The present $\sigma(60,+)$ curve and that by Kou et al. are normalized at $h\nu = 80$ eV. The two curves agree well between ~60 and 120 eV. With decreasing photon energy below ~60 eV the present curve starts to deviate upward from that by Kou et al. and the ratio of the two cross sections reaches ~2.5 at 25 eV. This discrepancy can be accounted for by the fact that the contamination of the second-order light brings about a serious distortion of the $\sigma(60,+)$ curve by Kou et al. at $h\nu = 40-60$ eV. In the present study correction of the $\sigma(60,z+)$ has been performed carefully by estimating the percentage of the second-order light. Reliability of our $\sigma(60,z+)$ in Figure 2a can be confirmed by comparison with previously published data of the total photoionization cross section $\sigma_T(60)$ of C_{60}. In Figure 2b closed circles indicate the sum of $\sigma(60,+)$, $\sigma(60,2+)$, and $\sigma(60,3+)$, which is approximately equivalent to $\sigma_T(60)$, while the dotted curve represents the $\sigma_T(60)$ curve observed by Reinköster et al.[14] and the dashed curve shows the total photoabsorption cross section calculated by Colavita et al.[16] These three curves are normalized at $h\nu = 100$ eV. Moreover, Figure 2b contains the absolute atomic cross section reported by Henke et al.,[24] that is, 60 times the total photoabsorption cross section of a C atom or 60 × σ(C). The curve of $\sigma(60,+) + \sigma(60,2+) + \sigma(60,3+)$ of the present study is in fair agreement with the published curves over an entire energy range, which provides tangible evidence for the validity of our analysis described in the Experimental Section. In contrast, neglecting the m/z dependence of the detection efficiency resulted in overestimation of $\sigma(60,2+)$ by Kou et al. and eventually rendered the sum of their cross sections, $\sigma(60,+) + \sigma(60,2+)$, unduly enhanced above 50 eV (see the solid curve in Figure 2b).

In Figure 2b, our data of $\sigma(60,+) + \sigma(60,2+) + \sigma(60,3+)$ are plotted in such a way that a summed value at $h\nu = 25$ eV accords with the total photoabsorption cross section of 407 Mb reported by Jaensch and Kamke[25] in 2000. These authors directly measured $\sigma_T(60)$ below 26 eV by monitoring the transmission of synchrotron radiation through a cell filled with C_{60} vapor. With the above normalization, our data in Figure 2b gives $\sigma_T(60) \sim 21$ Mb at $h\nu \sim 110$ eV, which is slightly smaller than 60 × σ(C) of 24.5 Mb at $h\nu = 108.5$ eV. Conversely $\sigma_T(60)$ of 114 Mb reported by Mori et al.[22] is 4.7 times as large as 60 × σ(C) because their evaluation was based essentially on the $\sigma(60,+) + \sigma(60,2+)$ curve by Kou et al. in Figure 2b. We are now trying to construct the $\sigma_T(60)$ spectrum over the visible to extreme UV region and to inspect the consistency of the calculated oscillator strength with the TKR sum rule, as have been performed by Berkowitz in 1999.[26]

Although the magnitude of $\sigma(60,+)$ by Kou et al. has been greatly revised upward in Figure 2a, the fine structures observed in their curve reappeared in the present $\sigma(60,+)$ spectrum, i.e., two peaks at 26 and 34 eV and flat area ranging 40−50 eV.[3,27] The 34 eV peak was also discernible on the $\sigma(60,2+)$ curve as a shoulder in Figures 2a and 3a. These structures originate from ionization via the shape resonances as single-electron excitation to vacant orbitals.[3,16] The electron in the initial valence orbital

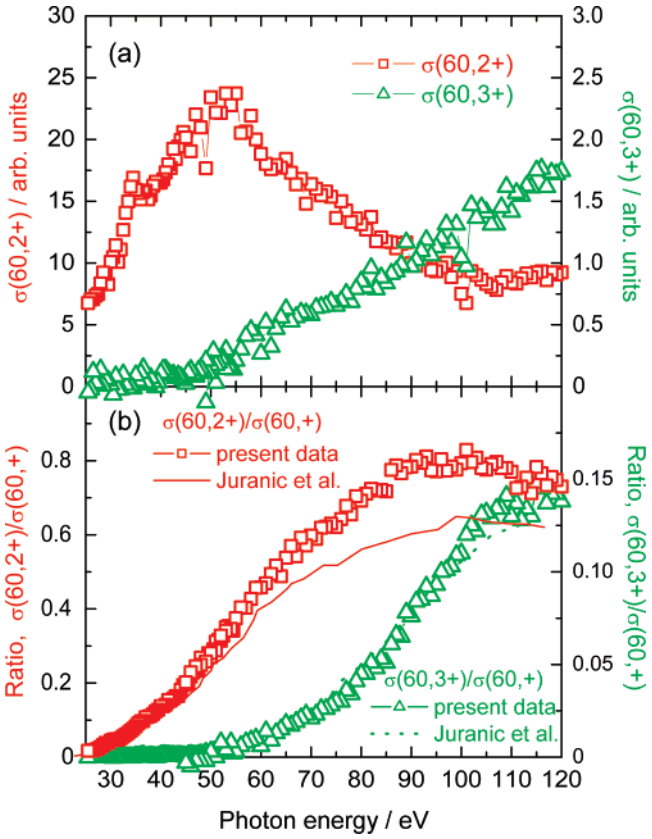

Figure 3. (a) Relative partial cross sections $\sigma(60,2+)$ and $\sigma(60,3+)$ for double and triple photoionization of C_{60}, respectively. (b) Ratios between the cross sections of multiple and single photoionization of C_{60}. The square and triangle symbols designate $\sigma(60,2+)/\sigma(60,+)$ and $\sigma(60,3+)/\sigma(60,+)$, respectively, of the present study. The solid and dotted curves indicate $\sigma(60,2+)/\sigma(60,+)$ and $\sigma(60,3+)/\sigma(60,+)$, respectively, reported by Juranic et al.[15]

has a high angular momentum, which is capable of generating a strong centrifugal barrier on the effective potential and a well inside the barrier. The ionized electron is trapped temporarily in this barrier and gives rise to resonance enhancement in the ionization probability at a certain photon energy.

Figure 3a shows the relative partial cross sections $\sigma(60,2+)$ and $\sigma(60,3+)$ for double and triple photoionization of C_{60}, respectively. The $\sigma(60,2+)$ is the same as that in Figure 2a but the ordinate is expanded. The $\sigma(60,2+)$ curve makes a broad maximum at ca. 50 eV, above which it monotonically descends, in agreement with[3] $\sigma(60,2+)$ reported by Kou et al. In contrast, $\sigma(60,3+)$ has an onset around 40 eV and steadily increases with $h\nu$. This onset energy is consistent with the published ionization potential[15,28] of 35.6 or 39.8 eV for the formation of C_{60}^{3+} from C_{60}. Figure 3b shows the ratio between $\sigma(60,2+)$ and σ (60,+) and that between $\sigma(60,3+)$ and $\sigma(60,+)$, respectively. Both the ratios increase with increasing $h\nu$, though the $\sigma(60,2+)/\sigma(60,+)$ curve reaches a saturated value of 0.78 at $h\nu \sim 85$ eV. The ratio $\sigma(60,3+)/\sigma(60,+)$ amounts to be 0.14 at 120 eV. Juranic et al. have measured cross-section ratios for double-to-single and triple-to-single photoionization[15] as a function of $h\nu$. Their results are represented by solid and dotted curves in Figure 3b. The curves of Juranic et al. agree well with those of the present study, particularly in the case of $\sigma(60,3+)/\sigma(60,+)$. A factor of 1.2 is needed to scale their curve of $\sigma(60,2+)/\sigma(60,+)$ to the present spectrum.

Partial Cross Sections for Single and Multiple Photoionization of C_{70}. The TOF mass spectra of the parent C_{70}^{z+} and fragment ions C_{70-2n}^{z+} ($n \geq 1$) produced from C_{70} are shown

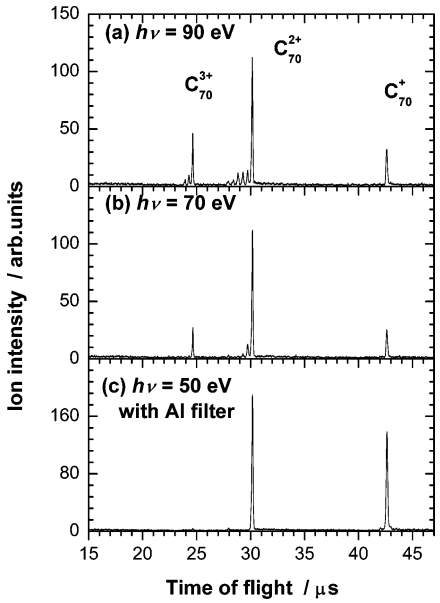

Figure 4. Time-of-flight mass spectra obtained by photoionization of C_{70} measured at three different photon energies. The signal intensity has been processed by neither normalization to the photon and molecular-beam fluxes nor correction of detection efficiencies of the MCP ion detector.

in Figure 4. The appearance $h\nu$ values of the ion yield curves for C_{70-2n}^{z+} are higher by 34 eV than the thermochemical thresholds for dissociative photoionization of C_{70}, leading to C_{70-2n}^{z+}.[7,29] These remarkably large kinetic shifts of the appearance energies have been interpreted in terms of statistical IVR in the primary C_{70}^{z+} ions and their sequential ejection of C_2 units, as discussed in detail in the previous paper.[7] From the experimental appearance energies of C_{70-2n}^{z+} we could evaluate the upper limits of the primary internal energies above which $C_{70-2n+2}^{z+}$ fragments cannot escape from further dissociating into $C_{70-2n}^{z+} + C_2$. These critical internal energies agreed well with the theoretical appearance internal energies of C_{70}^{z+} that corresponds to the threshold for the formation of C_{70-2n}^{z+}.[7]

Figure 5a shows the relative partial cross sections $\sigma(70,+)$ and $\sigma(70,2+)$ for single and double photoionization of C_{70}, respectively, that were calculated using eq 2. The solid and dashed curves in Figure 5a show $\sigma(70,+)$ and $\sigma(70,2+)$, respectively, reported by Kou et al.[3] At all photon energies $\sigma(70,2+)$ of the present study is smaller than that by Kou et al. because of the relation $\eta(C_{70}^{2+}) = 3.2\eta(C_{70}^{+})$. The present $\sigma(70,+)$ curve and that by Kou et al. are normalized at $h\nu =$ 80 eV. Both of the curves decrease with increasing $h\nu$, except in the lower energy side of the shape resonance peak at 34 eV. The present curve falls more steeply than that by Kou et al. To determine the $\sigma(70,+)$ curve, we closely examined the $h\nu$ dependence of the percentage of the second-order light of G2 (see Experimental Section). Moreover, we put a 100 nm thick aluminum foil in the path of the synchrotron radiation beam upstream the ionization region to suppress the second-order light. The $\sigma(70,+)$ curves obtained with and without the aluminum foil are found to behave similarly at $h\nu = 45-74$ eV if an appropriate correction of the second-order light is applied to the latter curve. We therefore suspect that $\sigma(70,+)$ by Kou et al. suffered from the contamination of the second-order light. Figure 5b shows the sum of $\sigma(70,+)$, $\sigma(70,2+)$, and $\sigma(70,3+)$, which is expected to be approximately equal to the total photoionization cross section $\sigma_T(70)$ of C_{70}. The present

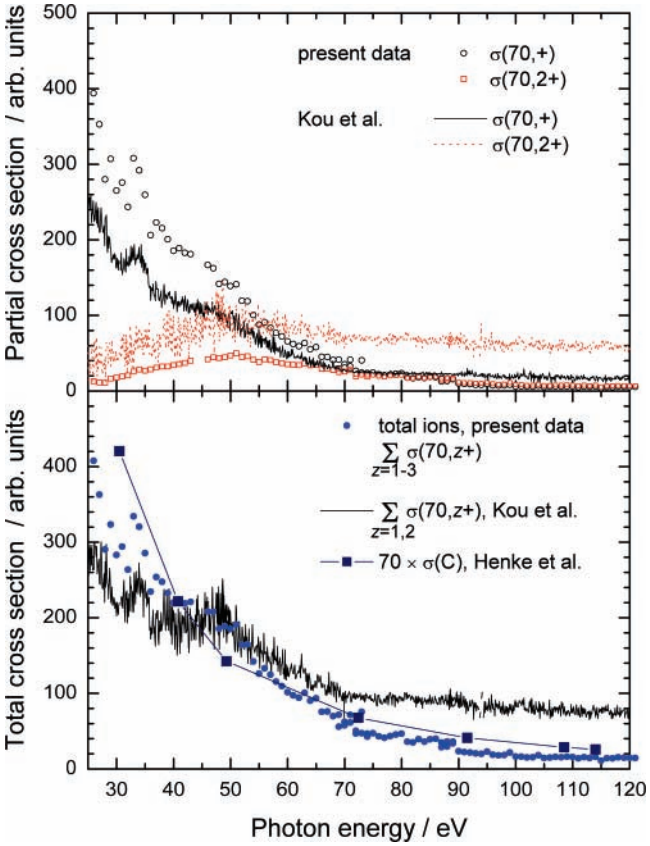

Figure 5. (a) Relative partial cross sections for single and double photoionization of C_{70}. The circle and square symbols designate $\sigma(70,+)$ and $\sigma(70,2+)$, respectively, of the present study. The solid and dotted curves indicate $\sigma(70,+)$ and $\sigma(70,2+)$, respectively, reported by Kou et al.[3] The present and previous $\sigma(70,+)$ curves are normalized at $h\nu = 80$ eV. (b) Closed circles indicate the total photoionization cross section $\sigma_T(70)$ of C_{70} determined in the present study. Solid curve, the sum[3] of $\sigma(70,+)$ and $\sigma(70,2+)$ by Kou et al.; closed squares, 70 times the total photoabsorption cross section of a C atom.[24]

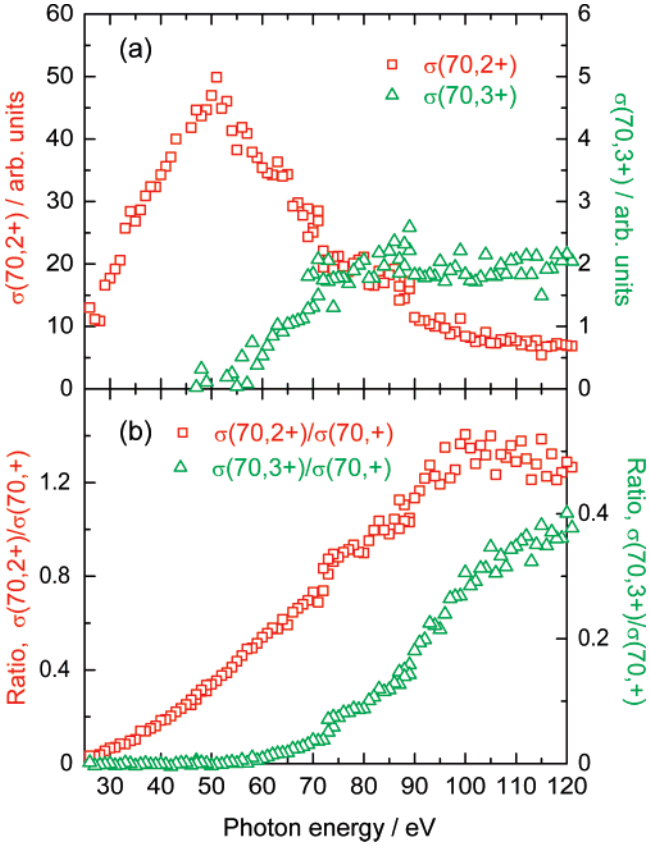

Figure 6. (a) Relative partial cross sections $\sigma(70,2+)$ and $\sigma(70,3+)$ for double and triple photoionization of C_{70}, respectively. (b) Ratios between the cross sections of multiple and single photoionization of C_{70}. The square and triangle symbols designate $\sigma(70,2+)/\sigma(70,+)$ and $\sigma(70,3+)/\sigma(70,+)$, respectively.

$\sigma_T(70)$ curve appears to change in harmony with the 70 times the total photoabsorption cross section of a C atom or 70 × σ(C).[24]

Figure 6a shows the relative partial cross sections $\sigma(70,2+)$ and $\sigma(70,3+)$ for double and triple photoionization of C_{70}, respectively. The $\sigma(70,2+)$ is the same as that in Figure 5a but the ordinate is expanded. The $\sigma(70,2+)$ curve peaks at ca. $h\nu = 50$ eV similarly to $\sigma(60,2+)$ in Figure 3a, whereas $\sigma(70,3+)$ starts to rise at around 50 eV and levels off above 80 eV. Figure 6b shows the ratios $\sigma(70,z+)/\sigma(70,+)$ with $z = 2$ and 3. The curve of $\sigma(70,2+)/\sigma(70,+)$ resembles that of $\sigma(60,2+)/\sigma(60,+)$ and converges to ~1.3 above 100 eV. The ratio $\sigma(70,3+)/\sigma(70,+)$ reaches 0.38 at 120 eV. Apparently, $s(70,z+)/\sigma(70,+)$ is larger than $s(60,z+)/\sigma(60,+)$ at any $h\nu$ position. The ratios of the partial cross sections evaluated from Figures 3b and 6b are summarized in Table 2.

TABLE 2: Ratios $\sigma(k,z+)/\sigma(k,+)$ between the Cross Sections for Multiple and Single Photoionization of Fullerenes[a]

	$\sigma(60,z+)/\sigma(60,+)$	$\sigma(70,z+)/\sigma(70,+)$
$z = 2$	0.78	1.3
$z = 3$	0.14	0.38

[a] Here, $k = 60$ or 70 specifies C_{60} or C_{70}, respectively. The ratios for $z = 2$ and 3 are estimated at $h\nu = 100$ and 120 eV, respectively.

Formation Mechanism of Multilply Charged Fullerene Ions. Colavita et al. have calculated the partial photoionization cross sections for valence electrons as a function of the photon energy using local density approximation Hamiltonian over an extended energy range.[16] Hence, we will discuss the formation mechanism of C_{60}^{2+} from C_{60} with the help of their results. Analogous mechanisms may hold for the formation of C_{70}^{2+} from C_{70}. The partial photoionization cross sections of Colavita et al. were characterized by the presence of many resonances up to about 40 eV above the respective photoionization thresholds. One can thus expect that these resonances should participate in the formation of C_{60}^{2+} below $h\nu \sim 65$ eV since the binding energies of deepest valence orbitals of C_{60} are located approximately from −24 to −28 eV. Among the reported partial cross sections the curve of photoionization of the $3g_g$ and $5h_g$ orbitals demonstrates pronounced broad resonances at $h\nu = 37$ and 50 eV. These resonances are considered to give rise to the peaks at 35 and 50 eV on the cross section curve of doubly charged ions in Figure 3a if we take account of the broadening of the theoretical peaks by many electron or vibrational effects. Colavita et al. ascribed the resonances at $h\nu = 37$ and 50 eV to promotion of the $3g_g$ and/or $5h_g$ electron to spherical standing waves inside the cavity of fullerene which have high angular momenta. The energies of the final orbitals are calculated from the binding energies[16] (−22.42 and −22.89 eV) of the $3g_g$ and $5h_g$ orbitals to be ~14 and ~27 eV, corresponding to the resonances at $h\nu = 37$ and 50 eV, respectively.

We can propose a possible pathway for the formation of C_{60}^{2+}, identifying the dominant features of the C_{60}^{2+} curve in Figure 3a with the above cavity resonances involving spherical standing waves. Let us assume that the cavity-resonance state

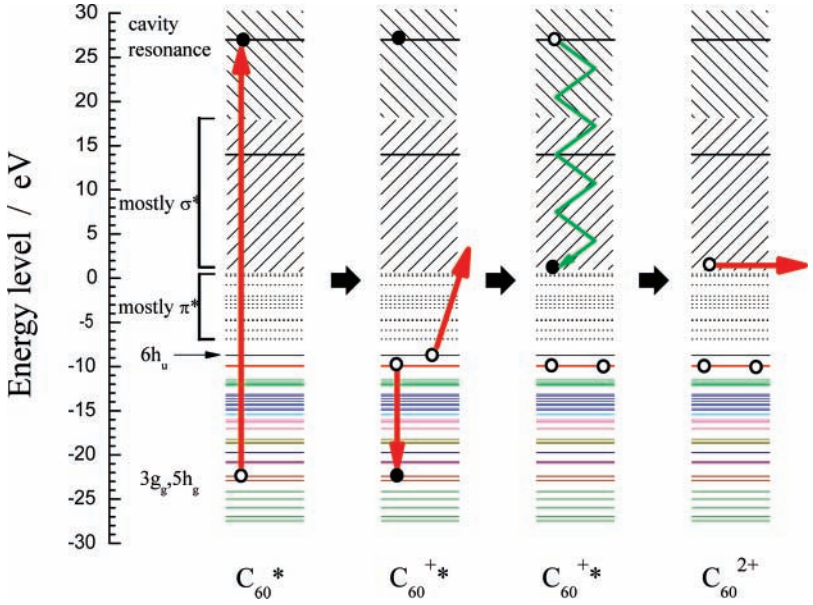

Figure 7. Schematic picture illustrating the decay mechanism of the cavity-resonance state formed by excitation of the $3g_g$ electron of C_{60}. Vibrationally excited C_{60}^{2+} can be produced by spectator Auger ionization, multiple internal conversion with intramolecular vibrational redistribution, and tunneling of the excited electron. Occupied and vacant orbitals are indicated by solid and dotted lines, respectively, and their binding energies are taken from refs 16 and 30, respectively.

is formed by promotion of the $3g_g$ or $5h_g$ electron when C_{60} absorbs a 50 eV photon (see Figure 7). Then spectator Auger ionization leads to C_{60}^{+}* in which the excited electron is still trapped inside the cavity. This excited state undergoes multiple conversion to other nearby cavity-resonance or shape-resonance states by transmitting a part of the electronic energy to numerous vibrational modes. Such conversion may occur consecutively until the excited electron is stabilized down to one of the low lying unoccupied orbitals of antibonding π^* or σ^* character near the threshold.[30] Thereby, the excess energy of at most ~27 eV is dissipated inside the fullerene cage. Finally, C_{60}^{2+} is produced by tunneling of the electron in the antibonding orbital. We believe this mechanism is most plausible below $h\nu \sim 65$ eV for the formation of C_{60}^{2+}.

Above $h\nu \sim 65$ eV single-electron excitation to cavity-resonance or shape-resonance states is improbable because the theoretical calculation[16] shows that partial photoionization cross sections are less dominated by these resonances. Instead, we should invoke neutral states with two electrons being excited. Here, two electrons can be excited to two antibonding unoccupied orbitals or to an antibonding orbital and an intracavity standing wave. Though Colavita et al. disregarded the contribution of such states, double-electron excitation is known to commonly occur for ordinary molecules at photon energies ≥20 eV above the photoionization threshold since electron correlations play an important role in such a high-energy region.[31] Both or either of the two holes at the valence orbitals experience spectator Auger decay to lead C_{60}^{+}* or C_{60}^{2+}*. In parallel with this Auger rearrangement, the two electrons primarily excited are stabilized down to low lying π^* or σ^* orbitals with transmitting the electronic energy to vibrational modes of C_{60}. Then C_{60}^{2+} and C_{60}^{3+} are produced from C_{60}^{+}* and C_{60}^{2+}*, respectively, if one of the excited electrons is ionized by tunneling.

In the present study we have observed that the partial cross section for double photoionization is comparable with that for single photoionization above $h\nu \sim 80$ eV as shown in Figure 3b. Obviously, C_{60}^{2+} produced from a double-electron excited state is stable with respect to direct dissociation, electronic predissociation, and Coulomb explosion into two singly charged fragments. It is likely that C_{70}^{2+} is expected to be more stable than C_{60}^{2+} for the following reasons. First, the rate of dissociation should decrease with decreasing average energy deposited to each vibrational mode through internal conversion and IVR. Second, the two holes created in C_{70}^{2+} can be delocalized over a larger space than those in C_{60}^{2+}. The relation $\sigma(70,z+)/\sigma(70,+) > \sigma(60,z+)/\sigma(60,+)$ ($z = 2$ and 3) in Table 2 may be interpreted in terms of more favorable charge delocalization in C_{70}^{z+} than in C_{60}^{z+}. Alternatively, the reason for this relation might lie in a higher density of cavity-resonance or shape-resonance states for C_{70}. The rate of double-electron excitation is expected to be very sensitive to the density of these states.

Conclusions

We experimentally determined the partial cross sections for single, double, and triple photoionization of C_{60} and C_{70} from the yield curves of individual ions, i.e., their signal count rate normalized to the photon flux and mass deposition rate of the thickness monitor. Close evaluation of the relative detection efficiency of the MCP ion detector and percentage of the second-order light allowed us to achieve reliable cross section curves in the $h\nu$ range of 25−120 eV for C_{60} and C_{70}. The validity of the present analysis was demonstrated by comparing the curve of the total photoionization cross section of C_{60} with the previous data published by other groups. In the present paper the partial cross-section curves for single and double photoionization of C_{70} are fully revised. Moreover, the curve for triple photoionization of C_{70} is newly proposed. We discussed possible formation mechanisms of multiply charged fullerene ions below and above $h\nu \sim 65$ eV, which are shown to be compatible with the $h\nu$ dependence of the ratios between the cross sections for double and single photoionization.

Acknowledgment. We are grateful to the members of the UVSOR for their help during the course of the experiments. This work has been supported by the Joint Studies Program (2004−2006) of the Institute for Molecular Science, by national funds appropriated for special research projects of the Institute for Molecular Science, by Grants-in-Aid for Scientific Research

(Grant Nos. 14340188, 18350016, and 17750023) from the Ministry of Education, Science, Sports, and Culture, Japan, and by a grant for scientific research from Research Foundation for Opto-Science and Technology.

References and Notes

(1) Hertel, I. V.; Steger, H.; de Vries, J.; Weisser, B.; Menzel, C.; Kamke, B.; Kamke, W. *Phys. Rev. Lett.* **1992**, *68*, 784.
(2) Xu, Y. B.; Tan, M. Q.; Becker, U. *Phys. Rev. Lett.* **1996**, *76*, 3538.
(3) Kou, J.; Mori, T.; Kumar, S. V. K.; Haruyama, Y.; Kubozono, Y.; Mitsuke, K. *J. Chem. Phys.* **2004**, *120*, 6005.
(4) Nenner, I.; Morin, P. In *VUV and Soft X-Ray Photoionization*; Becker, U., Shirley, D. A., Eds.; Plenum Press: New York, 1996; Chapter 9.
(5) Eland, J. H. D.; Schmidt, V. In *VUV and Soft X-Ray Photoionization*; Becker, U., Shirley, D. A., Eds.; Plenum Press: New York, 1996; Chapter 14.
(6) Kou, J.; Mori, T.; Kubozono, Y.; Mitsuke, K. *Phys. Chem. Chem. Phys.* **2005**, *7*, 119.
(7) Mitsuke, K.; Katayanagi, H.; Kou, J.; Mori, T.; Kubozono, Y. *Am. Inst. Phys. Conf. Proc.* **2006**, *811*, 161.
(8) Holland, D. M. P.; Codling, K.; West, J. B.; Marr, G. V. *J. Phys. B* **1979**, *12*, 2465.
(9) Twerenbold, D.; Gerber, D.; Gritti, D.; Gonin, Y.; Netuschill, A.; Rossel, F.; Schenker, D.; Vuilleumier, J.-L. *Proteomics* **2001**, *1*, 66.
(10) Gervasio, G.; Gerber, D.; Gritti, D.; Gonin, Y.; Twerenbold, D.; Vuilleumier, J.-L. *Nucl. Instrum. Methods Phys. Res., Sect. A* **2000**, *444*, 389.
(11) Krems, M.; Zirbel, J.; Thomason, M.; DuBois, R. D. *Rev. Sci. Instrum.* **2005**, *76*, 093305.
(12) Fraser, G. W. *Int. J. Mass Spectrosc.* **2002**, *215*, 13.
(13) Westmacott, G.; Frank, M.; Labov, S. E.; Benner, W. H. *Rapid Commun. Mass Spectrom.* **2000**, *14*, 1854.
(14) Reinköster, A.; Korica, S.; Prümper, G.; Viefhaus, J.; Godehusen, K.; Schwarzkopf, O.; Mast, M.; Becker, U. *J. Phys. B* **2004**, *37*, 2135.
(15) Juranic, P. N.; Lukic, D.; Barger, K.; Wehlitz, R. *Phys. Rev. A* **2006**, *73*, 042701.
(16) Colavita, P.; Alti, G. de; Fronzoni, G.; Stener M.; Decleva, P. *Phys. Chem. Chem. Phys.* **2001**, *3*, 4481.
(17) Ono, M.; Yoshida, H.; Hattori H.; Mitsuke, K. *Nucl. Instrum. Methods Phys. Res. A* **2001**, *467*−*468***,** 577.
(18) Mori, T.; Kou, J.; Ono, M.; Haruyama, Y.; Kubozono, Y.; Mitsuke, K. *Rev. Sci. Instrum.* **2003**, *74*, 3769.
(19) Yoshida, H.; Mitsuke, K. *J. Synchrotron Rad.* **1998**, *5*, 774.
(20) Bizau, J. M.; Wuilleumier, F. J. *J. Electron Spectrosc. Relat. Phenom.* **1995**, *71*, 205.
(21) Saito, N.; Suzuki, I. H. *Int. J. Mass Spectrom. Ion Proc.* **1992**, *115*, 157.
(22) Mori, T.; Kou, J.; Haruyama, Y.; Kubozono Y.; Mitsuke, K. *J. Electron Spectrosc. Relat. Phenom.* **2005**, *144*−*147*, 243.
(23) Mitsuke, K.; Mori, T.; Kou, J.; Haruyama, Y.; Kubozono, Y. *J. Chem. Phys.* **2005**, *122*, 064304.
(24) Henke, B. L.; Gullikson, E. M.; Davis, J. C. *At. Data Nucl. Data Tables* **1993**, *54*, 218.
(25) Jaensch, R.; Kamke, W. *Mol. Mater.* **2000**, *13*, 143.
(26) Berkowitz, J. *J. Chem. Phys.* **1999**, *111*, 1446.
(27) Kou, J.; Mori, T.; Ono, M.; Haruyama, Y.; Kubozono, Y.; Mitsuke, K. *Chem. Phys. Lett.* **2003**, *374*, 1.
(28) Scheier, P.; Dünser, B.; Wörgötter, R.; Lezius, M.; Robl, R.; Märk, T. D. *Int. J. Mass Spectrom. Ion Proc.* **1994**, *138*, 77.
(29) Matt, S.; Echt, O.; Wörgötter, R.; Scheier, P.; Klots, C. E.; Märk, T. D. *Int. J. Mass Spectrom. Ion Proc.* **1997**, *167/168*, 753.
(30) Saito, S.; Oshiyama, A. *Phys. Rev. Lett.* **1991**, *66*, 2637.
(31) Yoshida, H.; Mitsuke, K. *J. Chem. Phys.* **1994**, *100*, 8817.